

# Effect of austenite deformation temperature on Nb clustering and precipitation in microalloyed steel

E.V. Pereloma,<sup>a,b</sup> A.G. Kostryzhev,<sup>a,\*</sup> A. AlShahrani,<sup>a</sup> C. Zhu,<sup>c,d</sup> J.M. Cairney,<sup>c,d</sup>  
C.R. Killmore<sup>e</sup> and S.P. Ringer<sup>c,d</sup>

<sup>a</sup>*School of Mechanical, Materials and Mechatronic Engineering, University of Wollongong, NSW 2522, Australia*

<sup>b</sup>*UOW Electron Microscopy Centre, University of Wollongong, NSW 2519, Australia*

<sup>c</sup>*Australian Centre for Microscopy and Microanalysis, The University of Sydney, NSW 2006, Australia*

<sup>d</sup>*School of Aerospace, Mechanical and Mechatronic Engineering, The University of Sydney, NSW 2006, Australia*

<sup>e</sup>*BlueScope Steel Ltd., Five Islands Rd, Port Kembla, NSW 2500, Australia*

Received 20 October 2013; revised 21 November 2013; accepted 22 November 2013

Available online 1 December 2013

The effect of thermomechanical processing conditions on Nb clustering and precipitation in both austenite and ferrite in a Nb–Ti microalloyed steel was studied using electron microscopy and atom probe tomography. A decrease in the deformation temperature increased the Nb-rich precipitation in austenite and decreased the extent of precipitation in ferrite. Microstructural mechanisms that explain this variation are discussed.

© 2013 Acta Materialia Inc. Published by Elsevier Ltd. All rights reserved.

**Keywords:** Nb clustering; Precipitation; Steel; Atom probe tomography; Electron microscopy

The wide range of mechanical properties attainable in high-strength, low-alloy (HSLA) steels coupled with their relatively low cost are responsible for their high volume of production, which represents ~10% of the world's steel production. The high yield strengths of these steels (~550–600 MPa) arise through microalloying (<0.1 wt.%) of Nb, Ti and V. A vast amount of research [1,2] has been directed to understanding the mechanisms by which these microalloying elements modify the steel microstructure, and thereby influence the mechanical properties. At high temperatures, the microstructure of these steels is affected by the processes of recovery, recrystallization and grain boundary–particle interactions [1–5]. The microalloying elements retard austenite recrystallization via solute drag and/or particle pinning of grain boundaries, and this leads to austenite grain refinement. At low temperatures in ferrite, dislocation–particle interactions lead to precipitation strengthening [6]. One of the most protracted debates amongst researchers for the last 30 years has been the relative role of microalloyed solute atoms vs. the role of strain-induced precipitation on the kinetics of austenite recrystallization.

Much of this debate has been in the area of Nb-bearing HSLA steels [7]. Some authors consider that solute atoms are more effective in retarding recrystallization [4,8], while others argue that precipitates are more effective [9,10]. To obtain the desired overall microstructure requires a tuning of the grain size, dislocation substructure and precipitate dispersions, and this in turn requires that some of the thermomechanical processing (TMP) is conducted above and below the recrystallization temperature. In this work, we compare and contrast the distribution of Nb in a HSLA steel subjected to deformation in these two temperature regions. This analysis was carried out using atom probe tomography (APT), which has been proven to be an effective technique for acquiring information about the precise 3-D arrangement of the Nb atoms in the form of segregation, clustering and precipitation in steels [11,12].

A microalloyed steel produced by BlueScope Steel Ltd. containing 0.081C–1.20Mn–0.27Si–0.021Ni–0.019Cr–0.1Mo–0.016Cu–0.037Al–0.064Nb–0.021Ti–0.003V–0.001S–0.012P–0.0047 N (wt.%) was subjected to TMP using a Gleeble 3500 simulator [13]. The steel was firstly austenitized at 1250 °C for 300 s, and then given a roughing deformation strain of 0.35 at a strain rate of 5 s<sup>−1</sup> at 1100 °C. The samples were then cooled

\* Corresponding author. Tel.: +61 0242213034; fax: +61 0242213662; e-mail addresses: [kostryzhev@yahoo.com](mailto:kostryzhev@yahoo.com); [andrii@uow.edu.au](mailto:andrii@uow.edu.au)

at  $1\text{ }^{\circ}\text{C s}^{-1}$  to either 1075 or 825  $^{\circ}\text{C}$ , and deformed up to a strain of 0.75 at a strain rate of  $5\text{ s}^{-1}$ . After this, three cooling schedules were employed: (i) a water quench; (ii) cooling at  $1\text{ }^{\circ}\text{C s}^{-1}$  to 800  $^{\circ}\text{C}$  (above the austenite-to-ferrite transformation start temperature), followed by a water quench at  $\sim 160\text{ }^{\circ}\text{C s}^{-1}$ ; and (iii) cooling at  $1\text{ }^{\circ}\text{C s}^{-1}$  to 600  $^{\circ}\text{C}$  (in the ferrite temperature region), holding for 300 s, followed by air cooling to room temperature. As the microstructures formed on quenching were mainly martensitic with some lower bainite, it is assumed that no redistribution of substitutional elements has taken place. Thus, our use of APT provided insight into the distribution of alloying elements in austenite before the quench. Atom probe tips were prepared from the centre of the Gleeble samples perpendicular to the compression axis following a standard two-stage electropolishing procedure [14,15]. Atom probe data was collected on a Cameca Local Electrode Atom Probe (LEAP<sup>TM</sup>), operating at a temperature of 20 K and a pulse fraction rate of 20%. The data reconstruction was performed following the methodology described in Ref. [16]. Solute atom clustering and fine precipitation were identified and analysed using a maximum distance separation program provided by Dr. M.K. Miller, Oak Ridge National Laboratory, TN, USA. The Guinier radii,  $r_G$ , of clusters/fine carbides were calculated from radii of gyration ( $l_g$ ) data using the equation:  $r_G = \sqrt{(5/3) l_g}$  [14,15]. The determined cluster size takes into account the 57% detection efficiency and is based on the positions of all detected atoms. Thin foils for transmission electron microscopy (TEM) studies were prepared using tripod polishing method and ion milling. Field emission gun (FEG) TEM observations were carried out on a JEOL JEM-2200FS, using an accelerating voltage of 200 kV. Statistical analysis of precipitation was undertaken by scanning electron microscopy (SEM) using a JEOL 7001F FEG microscope operating at 5 kV, which allowed analysis of particles down to 20 nm in size.

A summary of precipitate number density distributions in samples studied using SEM is given in Figure 1. As both series of samples were subjected to the same austenitizing and roughing conditions, the distributions of coarse  $>70\text{ nm}$  TiN and (Ti,Nb)(C,N) particles are similar, and therefore are not a point for discussion here. On cooling below 1100  $^{\circ}\text{C}$ , which was estimated to be the dissolution temperature of NbC [17], the formation of precipitates was expected. This process can be accelerated by deformation [18], as crystal defects (dislocation nodes and tangles) provide additional heterogeneous nucleation sites for precipitation. However,

1075  $^{\circ}\text{C}$  was too high a deformation temperature to result in strain-induced precipitation. On the contrary, after deformation at 825  $^{\circ}\text{C}$  strain-induced precipitation occurred. Analysis of particle number density distributions is consistent with this (Fig. 1). After deformation at 1075  $^{\circ}\text{C}$  the number of  $<70\text{ nm}$  particles did not vary significantly during cooling to 800  $^{\circ}\text{C}$  in the austenite temperature region (Fig. 1a), which indicates the absence of strain-induced precipitation. After deformation at 825  $^{\circ}\text{C}$  the number density of  $<70\text{ nm}$  particles increased from  $0.38$  to  $0.93\text{ }\mu\text{m}^{-2}$ , i.e. by 2.4 times, during cooling in austenite (Fig. 1b), which indicates strain-induced precipitation. In addition, the particle area fraction in the samples quenched from 800  $^{\circ}\text{C}$  was about 50% higher for the 825  $^{\circ}\text{C}$  TMP schedule compared to that for the 1075  $^{\circ}\text{C}$  schedule ( $3.1 \times 10^{-3}$  vs.  $1.8 \times 10^{-3}$ ). This precipitation behaviour should have resulted in a larger amount of Nb retained in the austenite solution for the 1075  $^{\circ}\text{C}$  TMP schedule compared to that for the 825  $^{\circ}\text{C}$  schedule, which would lead to a variation in ferrite precipitation. Thus, during holding in ferrite after deformation at 1075  $^{\circ}\text{C}$  the number density of  $<70\text{ nm}$  particles increased from  $0.36\text{ }\mu\text{m}^{-2}$  (at 800  $^{\circ}\text{C}$ ) to  $1.44\text{ }\mu\text{m}^{-2}$  (at 600  $^{\circ}\text{C}$ ), i.e. by 4 times. During holding in ferrite after deformation at 825  $^{\circ}\text{C}$  the number density of  $<70\text{ nm}$  particles increased from  $0.93\text{ }\mu\text{m}^{-2}$  (at 800  $^{\circ}\text{C}$ ) to  $1.15\text{ }\mu\text{m}^{-2}$  (at 600  $^{\circ}\text{C}$ ), i.e. by only 24%. The particle area fraction in the samples deformed at 825  $^{\circ}\text{C}$  increased in ferrite by only  $0.1 \times 10^{-3}$  (with respect to the 800  $^{\circ}\text{C}$  quenched condition), reaching  $3.2 \times 10^{-3}$ , while in the samples deformed at 1075  $^{\circ}\text{C}$  it more than doubled (with respect to the 800  $^{\circ}\text{C}$  quenched condition), reaching  $4.7 \times 10^{-3}$ . These indicate a much more pronounced precipitation in ferrite following deformation at 1075  $^{\circ}\text{C}$ , compared to that at 825  $^{\circ}\text{C}$ . Analysis of the orientation relationships between the NbC and the ferrite matrix for all the TMP schedules revealed (Fig. 2) that some fine precipitates exhibited the Baker–Nutting orientation relationship  $(001)\text{NbC} // (001)\alpha$ ,  $[010]\text{NbC} // [110]\alpha$  [19], which indicates they precipitated in ferrite, whereas others did not show these orientations (Fig. 2b), confirming their origin in austenite.

Table 1 shows information about clusters of atoms measured using APT, which is able to resolve finer features than the SEM and TEM studies. After deformation at 1075  $^{\circ}\text{C}$  Nb–C clusters were not observed, with only 2–8 Nb atom clusters being present [13]. On the contrary, after deformation at 825  $^{\circ}\text{C}$  a relatively high

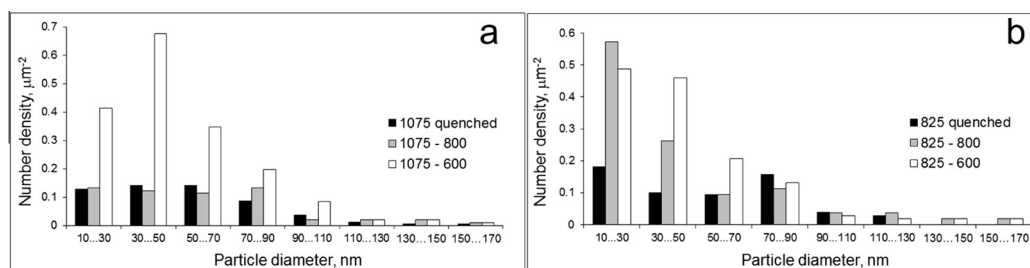
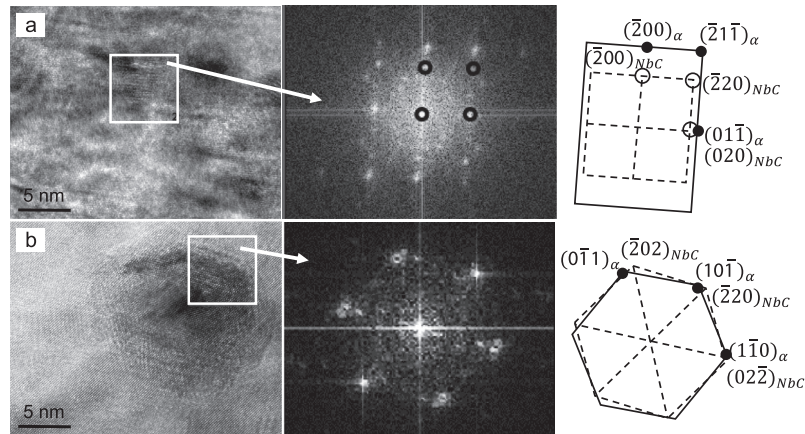


Fig. 1. Nb-rich precipitate number density distributions after various cooling schedules for samples deformed at (a) 1075  $^{\circ}\text{C}$  and (b) 825  $^{\circ}\text{C}$ .



**Fig. 2.** Representative high-resolution TEM images and corresponding diffraction patterns of NbC (a) with Baker–Nutting orientation relationship and (b) without an orientation relationship to ferrite.

**Table 1.** Characterization of Nb–C clusters/fine precipitates after various TMP schedules.

TMP condition	C, at.%	Nb, at.%	Fe, At.%	$r_G$ , nm	Cluster size, number of atoms	Number density, $\times 10^5 \mu\text{m}^{-3}$
1075–800	$84.4 \pm 8.7$	$8.1 \pm 5.1$	$5.3 \pm 4.3$	$1.7 \pm 0.2$	20–31	0.12
1075–600	$70.0 \pm 6.0$	$23 \pm 5.0$	$6.6 \pm 2.2$	$2.8 \pm 1.3$	20–580	0.6
825	$83.2 \pm 7.2$	$15.7 \pm 7$	$1.1 \pm 1.1$	$2.3 \pm 0.2$	23–28	0.4
825–800	$67.5 \pm 7.2$	$27.8 \pm 7$	$4.6 \pm 2.4$	$2.3 \pm 1.1$	20–758	0.6
825–600	$66.8 \pm 5.4$	$24.6 \pm 5$	$8.0 \pm 2.6$	$2.8 \pm 1$	20–601	0.34

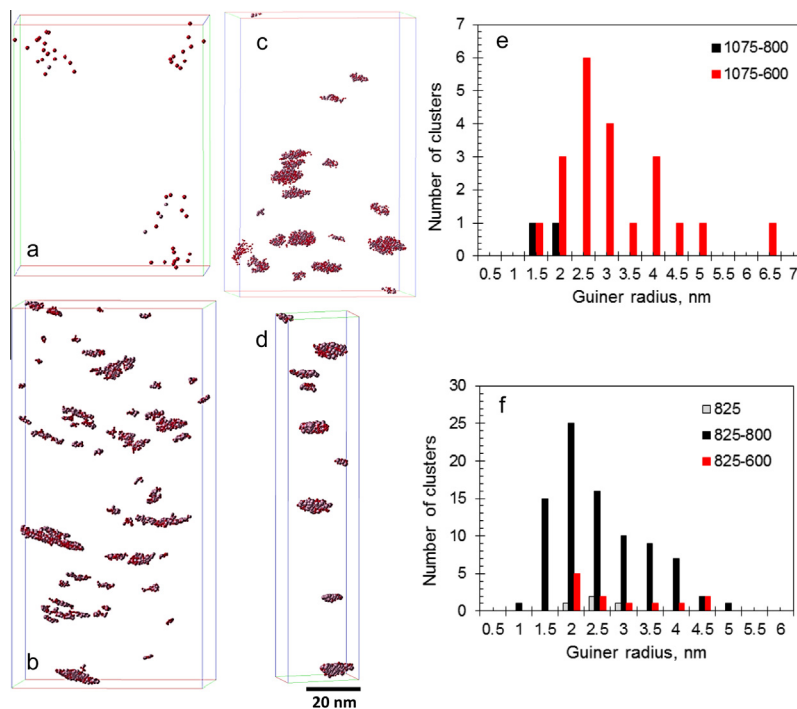


**Fig. 3.** Selected APT maps showing Nb–C clusters after quenching from 800 °C following deformation at (a) 1075 °C and (b) 825 °C, and after holding at 600 °C following deformation at (c) 1075 °C and (d) 825 °C; (e) and (f) are cluster size distributions for 1075 and 825 °C deformation temperature TMP schedules.

number density of Nb–C clusters precipitated (Table 1). This could be a result of both the longer cooling time after roughing to 825 °C, compared to that to 1075 °C, and a higher dislocation density after a lower deformation

temperature (825 °C vs. 1075 °C), which led to an increase in the number of nucleation sites for clusters. After cooling in austenite to 800 °C the Nb–C cluster number density was five times higher following deformation at

825 °C, compared to that following deformation at 1075 °C (Table 1, Fig. 3a,b), which indicates a much higher clustering rate in austenite for the lower deformation temperature schedule. As a result of an increased clustering and precipitation in austenite a matrix depletion in Nb might be expected following deformation at 825 °C, which would lead to the retardation of precipitation in ferrite for this condition. Thus, after holding at 600 °C the number density and cluster size of the Nb–C clusters increased from the 1075–800 to 1075–600 TMP condition (Table 1, Fig. 3c) and decreased from the 825–800 to 825–600 TMP condition (Table 1, Fig. 3d). A larger number of smaller clusters was observed for the 1075–600 TMP condition, compared to that for the 825–600 TMP condition (Fig. 3e and f). These results indicate a higher clustering rate in ferrite following deformation at higher temperature and, together with the analysis of particle behaviour (Fig. 1), growth of previously formed clusters following deformation at a lower temperature. All of the observed clusters were significantly enriched in C (Table 1), which indicates faster clustering of C atoms, probably on pre-existing Nb atom clusters [13], corresponding to a higher rate of diffusion of C atoms in austenite compared to Nb. However, there is a 20–40% overestimation of C concentration in fine clusters due to the deficiency of the envelope method [20]. During clustering in ferrite the Nb content in clusters increased following deformation at 1075 °C, but did not vary significantly for the samples deformed at 825 °C, which could indicate a higher Nb clustering rate in ferrite due to a higher Nb content remaining in the matrix after a higher deformation temperature. The composition of some coarser clusters approached stoichiometry (50/50) for the NbC particles. It is possible that these clusters serve as the precursor for NbC particles.

In summary, this study of Nb clustering and precipitation in a microalloyed steel has shown that a decrease in deformation temperature in austenite increases the rate of clustering and precipitation in austenite as a result of a slow dislocation annihilation rate and an increased number of cluster/precipitate nucleation sites. Conversely, the precipitation and clustering decreased in ferrite, following depletion of Nb from the matrix. While increased austenite precipitation has desirable effects arising from enhanced retardation of recrystallization and refined grain size, reduced ferrite precipitation may lead to a decrease in ferrite strengthening.

This work was financially supported by the Australian Research Council (LP110100231).

- [1] Microalloying 95: Proceedings of the International Conference Microalloying 95, 11–14 June 1995, Pittsburgh, PA, Iron and Steel Society Inc., 1995.
- [2] M. Korchynsky, in: Proceedings of Int. Symposium on Steel for Fabricated Structures, 1–4 November 1999, Cincinnati, OH, pp. 139–145.
- [3] L.Q. Ma, Z.Y. Liu, S.H. Jiao, X.Q. Yuan, D. Wu, J. Iron Steel Res. Int. 15 (2008) 31–36.
- [4] C.L. Miao, C.J. Shang, H.S. Zurob, G.D. Zhang, S.V. Subramanian, Metall. Mater. Trans. A 43 (2012) 665–676.
- [5] B. Dutta, E.J. Palmiere, C.M. Sellars, Acta Mater. 49 (2001) 785–794.
- [6] T. Gladman, The Physical Metallurgy of Microalloyed Steels, The Institute of Materials/Cambridge University Press, Cambridge, 1997.
- [7] A.J. DeArdo, Int. Mater. Rev. 48 (6) (2003) 371–402.
- [8] O. Kwon, A.J. DeArdo, Acta Metall. Mater. 39 (4) (1991) 529–538.
- [9] S. Vervynck, K. Verbeken, P. Thibaux, Y. Houbaert, Mater. Sci. Eng. A 528 (2011) 5519–5528.
- [10] C.R. Hutchinson, H.S. Zurob, C.W. Sinclair, Y.J.M. Brechet, Scr. Mater. 59 (2008) 635–637.
- [11] E.V. Pereloma, I.B. Timokhina, K. Russell, M. Miller, Scr. Mater. 54 (2006) 471–476.
- [12] Y. Xie, T.X. Zheng, J.M. Cairney, H. Kaul, J.G. Williams, C.C. Killmore, S.P. Ringer, Scr. Mater. 66 (2012) 710–713.
- [13] A.G. Kostyryzhev, A. AlShahrani, C. Zhu, S.P. Ringer, E.V. Pereloma, Mater. Sci. Eng. A 581 (2013) 16–25.
- [14] B.G. Gault, M.P. Moody, J.M. Cairney, S.P. Ringer, Atom Probe Microscopy, Springer, New York, 2012.
- [15] M.K. Miller, Atom Probe Tomography: Analysis at the Atomic Level, Springer Verlag, New York, 2000.
- [16] M.P. Moody, B. Gault, L.T. Stephenson, D. Haley, S.P. Ringer, Ultramicroscopy 109 (2009) 815–824.
- [17] B. Soenen, S. Jacobs, C. Klinkenberg, in: Proc. Materials Solutions Conference, 7–9 October, Columbus, OH, 2002, pp. 16–24.
- [18] B. Dutta, C.M. Sellars, Mater. Sci. Technol. 3 (1987) 197–206.
- [19] R.G. Baker, J. Nutting, Precipitation Processes in Steel, Special Report 64, Iron and Steel Institute, London, 1959.
- [20] E.V. Pereloma, M.K. Miller, I.B. Timokhina, Metall. Mater. Trans. A 39A (2008) 3210–3216.